Scripta Materialia 119 (2016) 55–59

Contents lists available at ScienceDirect

Scripta Materialia

journal homepage: www.elsevier.com/locate/scriptamat

Regular Article

Enhancing fracture toughness of nanotwinned austenitic steel by thermal annealing

L. Xiong [a], Z.S. You [a,b], L. Lu [a,*]

[a] Shenyang National Laboratory for Materials Science, Institute of Metal Research, Chinese Academy of Sciences, 72 Wenhua Road, Shenyang 110016, PR China
[b] Herbert Gleiter Institute of Nanoscience, Nanjing University of Science and Technology, 200 Xiaolingwei Street, Nanjing 210094, PR China

ARTICLE INFO

Article history:
Received 2 February 2016
Received in revised form 24 March 2016
Accepted 24 March 2016
Available online 13 April 2016

Keywords:
Dynamic plastic deformation
Austenitic stainless steel
Nanotwins
Fracture toughness
Thermal annealing

ABSTRACT

The fracture behavior was investigated of a 316L austenitic stainless steel with heterogeneously distributed nanotwin bundles, prepared by dynamic plastic deformation and subsequent annealing at different temperatures. The results indicate that the controlled annealing causes a slight decrease in the strength, but remarkably improves the fracture resistance, and therefore enhances the strength–toughness synergy. The toughness enhancement is attributable to the formation of recovered sub-micron-sized and recrystallized micron-sized grains postponing crack nucleation and to the remnant nanotwin bundles arresting crack propagation.

Austenitic stainless steels (SS) are widely used in engineering applications due to their excellent corrosion resistance and good formability [1]. But their low yield strengths in general limit the applications as energy efficient structural components [2]. Grain refinement by severe plastic deformation has attracted considerable attention to develop high strength steels [3–5]; however, the strength increment by this method is always accompanied with dramatic reduction in ductility and fracture toughness [5–7]. The reduced fracture toughness has an important bearing on the suppression of dislocation activities within the nanoscale tiny grains [7–9], and on the fact that the numerous large angle grain boundaries (GBs) in three-dimensional network can directly act as micro-void nucleation sites and crack extension paths [10,11]. Therefore, structural reliability and hence potential engineering applications of nanograined components are still seriously restricted by their limited damage tolerance.

By contrast, two-dimensional coherent twin boundaries (TBs) at the nanometer scale are more resistant to crack nucleation and propagation, while maintaining a significant strengthening capability [12–15]. For instance, by introducing bundles of nanoscale deformation twins into a matrix of nanograins, Qin et al. discovered that the nanotwin bundles could enhance the crack growth resistance by triggering the formation of coarse/deep dimples [16,17]. However, the presence of a large volume fraction of nanograins in the deformed samples still limits the crack initiation toughness, since micro-cracks easily nucleate and coalesce in the nanograined matrix. To solve this problem, controlled thermal treatment to modify the nanograined microstructure, which has been recognized to be an effective approach to deal with the strength–ductility trade-off relationship [18,19], can be a feasible strategy.

For the case of austenitic steels, it has been demonstrated that dynamic plastic deformation (DPD) in conjunction with optimized thermal annealing to produce a mixed structure consisting of nanotwinned and recrystallized austenitic grains could bring about a good combination of high strength and large tensile ductility [20,21]. However, there is still a lack of fracture mechanics evaluation on the damage tolerance of this unique material, which is highly required for engineering applications. In this work, the fracture behavior of the nanotwinned austenitic 316L SS was investigated, majorly aiming at evaluating the contributions of nanotwin bundles and recrystallized grains to the fracture toughness, and at exploring the underlying strengthening and toughening mechanisms.

The used 316L SS and the DPD treatment in this work are identical to those in Refs. [21,22]. Cylindrical coarse-grained samples, 12 mm in diameter and 16 mm in height, were subjected to repeated DPD treatments up to a total true strain of 1.6. The strain is defined as $\varepsilon = \ln(h_i/h_f)$, where h_i and h_f are the initial and final thickness of the treated sample. In order to further modify the microstructure, the as-DPD disk samples were annealed at 710–730 °C for 20 min and then water-quenched. Uniaxial tensile tests were performed on an Instron 5848 microtester (2 kN load capacity) at a strain rate of 3×10^{-3} s^{-1} at room temperature, using dog bone-shaped samples with a gage length of 5 mm. A contactless MTS LX300 laser extensometer was used to accurately measure the imposed strain upon loading.

* Corresponding author.
E-mail address: llu@imr.ac.cn (L. Lu).

http://dx.doi.org/10.1016/j.scriptamat.2016.03.024
1359-6462/

In order to evaluate the fracture toughness, miniaturized single edge-notched specimens with a thickness of 2 mm, a width of 4 mm, and a span distance of 16 mm were machined from the as-DPD and thermally treated disks, with the thickness direction corresponding to that of the DPD disk. The crack propagation direction is parallel to the radial direction of the disk, while the propagation plane is normal to the tangential direction. The specimens were first notched to a depth of ~800 μm by electrical discharge machining, and then pre-cracked under cyclic bending to an original crack length a_0 of ~2 mm. The pre-cracked specimens were finally monotonically bent to extend the crack at a constant displacement rate of 0.3 mm min^{-1} on the Instron 5848 microtester. During the test, the instantaneous crack length was monitored using the direct current potential drop method. With the synchronously recorded force P, load-line displacement v and crack extension Δa, the elastic–plastic fracture toughness (critical J-integral) could be determined from the J-integral resistance curves calculated based on the recommendations of the ASTM E1820-11 [23].

The microstructure was characterized by field emission gun scanning electron microscopy (SEM) in a FEI Nova NanoSEM 430 microscope and by transmission electron microscopy (TEM) using a JEOL 2010 microscope operated at 200 kV. Electron backscatter diffraction (EBSD) measurements and analysis were performed using the HKL channel 5 software suite. The fracture surfaces were examined by the SEM with secondary electron imaging, and by the Olympus LEXT OLS4000 confocal laser scanning microscope (CLSM) to determine the three-dimensional fracture topography.

Fig. 1a shows the typical cross-sectional microstructure of the as-DPD sample, which is spatially heterogeneous and is characterized by rhombic bundles of nanoscale deformation twins embedded in a matrix of nano-sized grains. The nanotwin bundles with longitudinal length ranging from several to tens of micrometers are remnants surviving from the extensive localized shear deformation in various directions. Closer TEM observations reveal a high density of dislocations accumulated along the TBs (Fig. 1b), characteristic of deformation twins. The statistical results indicate that the nanotwin bundles with a mean twin/matrix thickness of ~16 nm take up a total volume fraction of ~26%, with the balance being occupied by the nanograins. Most of the nanograins are generated inside the shear bands through the fragmentation and rotation of the twin/matrix lamellae, and hence are slightly elongated with an average transverse size of ~30 nm and a mean longitudinal size of ~80 nm.

Additional thermal annealing at 710–730 °C leads to substantial variations in the deformed microstructure. Fig. 1c shows the typical microstructure of the DPD sample annealed at 720 °C for 20 min. Obviously, nano-sized grains are much less stable due to the high stored energy comparing to nanotwinned structures, and hence partial recrystallization preferentially occurs in the nanograined areas to convert some of them to micron-sized recrystallized grains that are visible under the SEM observations. The EBSD measurements (Fig. 1f) reveal the presence of large angle misorientations between the recrystallized grains and the formation of the annealing twins inside. Due to the relatively low annealing temperatures, some deformed nano-grains are just recovered and become dislocation-free. These recovered sub-micron-sized grains usually surround the nanotwinned bundles, as shown in closer TEM observation (Fig. 1d). After the thermal annealing, there is no significant change in the volume fraction or the average twin/matrix thickness of the nanotwin bundles, due to their low interface energy and high thermal stability [24]. However, a large fraction of dislocations accumulated at TBs annihilates after the annealing (Fig. 1e). The statistical results of the microstructure for the as-DPD and the annealed DPD samples are summarized in Table 1.

The representative tensile engineering stress–strain curves for the as-DPD and the thermally treated samples are shown in Fig. 2. DPD to $\varepsilon = 1.6$ substantially elevates the yield strength σ_y up to 1366 MPa and the ultimate tensile strength σ_{uts} to 1416 MPa. However, it also dramatically reduces the tensile ductility. After the annealing treatments, the strengths (both σ_y and σ_{uts}) slightly drop due to the reduction in dislocation density and moderate grain coarsening. In return, an

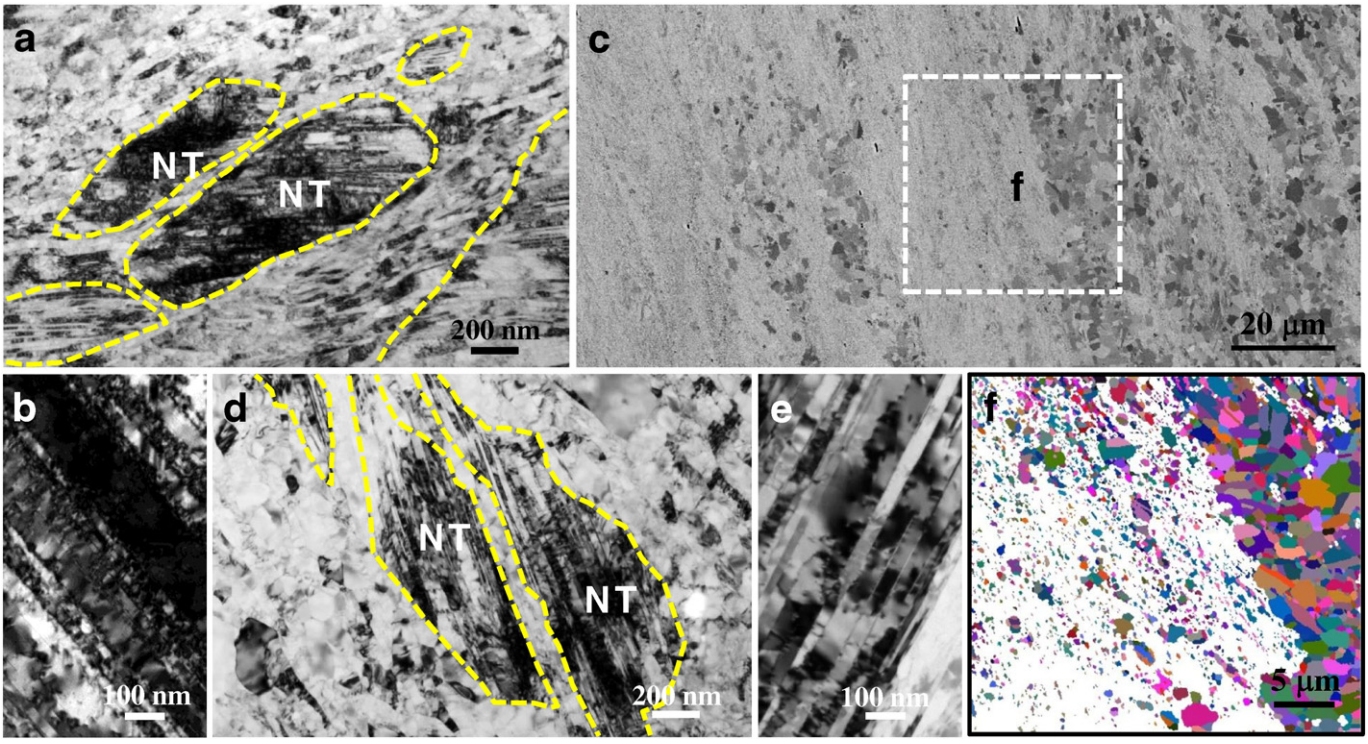

Fig. 1. (a) Cross-sectional microstructure of the as-DPD 316L SS, showing the nanotwin bundles embedded in a nanograin matrix; (b) closer TEM observation on the deformation twins with a high density of accumulated dislocations; (c) SEM image of the cross-sectional microstructure of the 720 °C annealed DPD sample, showing some recrystallized micron-sized grains; (d) closer TEM observations of the unresolved areas in (c), displaying the nanotwin bundles surrounded by equiaxed sub-micron grains; (e) TEM image of annealed nanotwins with a relatively low density of dislocations; (f) EBSD map of the selected area in (c), indicating the presence of high angle grain boundaries and annealing twins in the recrystallized grains.